Biosensors and Bioelectronics 284 (2025) 117566

Contents lists available at ScienceDirect

Biosensors and Bioelectronics

journal homepage: www.elsevier.com/locate/bios

Plasma-based ultrasensitive detection of *Mycobacterium tuberculosis* ESAT6/CFP10 fusion antigen using a CRISPR-driven aptamer fluorescence testing (CRAFT)

Siyuan Liu [a], Guohui Xiao [a], Peixuan Li [b], Yating Xu [a], Xinhao Fan [b], Lin Tian [a], Su Zhang [a], Guoliang Zhang [a,*]

[a] National Clinical Research Center for Infectious Diseases, Shenzhen Third People's Hospital, Southern University of Science and Technology, Shenzhen, 518112, PR China

[b] Shenzhen Branch, Guangdong Laboratory for Lingnan Modern Agriculture & Genome Analysis Laboratory of the Ministry of Agriculture, Agricultural Genomics Institute at Shenzhen, Chinese Academy of Agricultural Sciences, Shenzhen, 518000, PR China

ARTICLE INFO

Keywords:
Mycobacterium tuberculosis
Aptamer
ESAT6/CFP10
CRISPR
Plasma

ABSTRACT

Tuberculosis (TB) screening in clinical diagnosis is challenging due to issues such as sputum dependence, time-consuming procedures, and high costs. In this study, we introduce a CRAFT (CRISPR-Driven Aptamer Fluorescence Testing), an aptamer-based CRISPR/Cas12a assay designed for the rapid and sensitive detection of *Mycobacterium tuberculosis* (Mtb) antigens from peripheral blood. Aptamer 3 (Ap3) and the aptamer-mediated probe (Aptamer-blocker 3–7) were selected through the Systematic Evolution of Ligands by Exponential Enrichment (SELEX). Ap3 demonstrated a dissociation constant (*Kd*) of 8.3E-7 M with the ESAT6/CFP10 fusion proteins (EC proteins), which are produced during the replicative phase of Mtb. Upon labeling the EC proteins with Aptamer-blocker 3–7 (Ap-blocker 3–7) probe, single-stranded DNA (ssDNA) blocker 3–7 was released, thereby completing the process for RPA-based CRISPR/Cas12a fluorescence detection. After optimizing multiple parameters, CRAFT achieved a detection limit of 0.1 ag/mL EC proteins (equivalent to 3 protein particles per mL) within 120 min from plasma sample to result. The method was validated with 86 clinical plasma samples confirmed the method's high diagnostic accuracy for Mtb infection (sensitivity: 97.1 %, 95 % confidence interval (CI) [0.849–0.998]); specificity: 98.0 %, 95 % CI [0.897–0.999]), supporting its utility in early therapeutic evaluation of tuberculosis management.

1. Introduction

Tuberculosis (TB) remains a significant global health threat (Ehrt et al., 2018), with an estimated 10.6 million new cases and 1.3 million deaths reported in 2022 alone (Bagcchi, 2023). Timely and accurate diagnosis of live *Mycobacterium tuberculosis* (Mtb), the causative agent of TB, is crucial for effective disease management and control. However, conventional methods for Mtb detection, such as culture or GeneXpert, suffer from sputum dependence, time-consuming (Mtb culture taking more than two weeks), and requiring large instruments (Boehme et al., 2010, 2011). Furthermore, GeneXpert cannot differentiate between live and dead bacteria, greatly limits its predictive role in front-line clinical practice (Denkinger et al., 2014; MacLean et al., 2020). Therefore, there is an urgent need for rapid and accurate diagnostic approaches that can effectively address the challenges of diagnosing live Mtb in resource-limited conditions.

Aptamers are short, single-stranded nucleic acid molecules, either DNA or RNA, that possess a unique three-dimensional structure and exhibit high affinity and specificity for binding to target molecules, including proteins, small molecules, and pathogens (Song et al., 2013; Vinkenborg et al., 2011). In diagnostics, aptamers can serve as molecular probes for the detection and quantification of biomarkers or pathogens (Shi et al., 2024). For example, Aptamer-based electrochemical biosensors have shown considerable potential in the early-stage detection of Mtb antigens, specifically the MPT64 antigen, with a detection range from 0.02 to 1000 pg/mL (Li et al., 2018). However, aptamer exhibit limitations in relatively low binding affinities, ranging from picomolar to micromolar (Acquah et al., 2020), and can only detect 600

* Corresponding author.
E-mail address: zhanggl2020@mail.sustech.edu.cn (G. Zhang).

https://doi.org/10.1016/j.bios.2025.117566
Received 18 March 2025; Received in revised form 29 April 2025; Accepted 7 May 2025
Available online 8 May 2025
0956-5663/© 2025 Elsevier B.V. All rights are reserved, including those for text and data mining, AI training, and similar technologies.

CFU/mL of *Salmonella typhimurium* even combined with gold nanoparticle-modified screen-printed carbon electrodes and supporting equipment (Labib et al., 2012). Enhancing aptamer sensitivity through combination with other methods, such as PCR-free systems, can facilitate easier operation and cost-effectiveness, especially in resource-limited areas or during public health emergencies (Yang et al., 2023a).

The Clustered Regularly Interspaced Short Palindromic Repeats (CRISPR) technology has emerged as a powerful tool for nucleic acid diagnostics in diseases such as TB and SARS-CoV-2, owing to its simplicity, versatility, and high sensitivity (Joung et al., 2020; Tian et al., 2024; Xiao et al., 2020; Yang et al., 2023b). Notably, CRISPR achieves single-copy sensitivity for target genes when combined with isothermal amplification (Ai et al., 2019; Broughton et al., 2020; Gootenberg et al., 2017; Liu et al., 2021). However, the successful implementation of highly sensitive CRISPR diagnostic assays relies on the optimal enrichment of target genes and the efficient performance of guide RNAs (gRNAs), which must precisely recognize and bind to the target sequences. In CRISPR/Cas12a detection, gRNAs selectively target Mtb nucleic acid sequences that have been amplified using Recombinase Polymerase Amplification (RPA) or Polymerase Chain Reaction (PCR). Subsequently, the Cas12a enzyme is activated, resulting in the *cis*-cleavage of target double-stranded DNA (dsDNA) or single-stranded DNA (ssDNA) in clinical genome samples. Following *cis*-cleavage, Cas12a exhibits *trans*-cleavage activity, which facilitates the cleavage of untargeted ssDNA fragments containing fluorophore-quencher (FQ-ssDNA). This cleavage generates observable fluorescence that can be detected visually (Liu et al., 2021; Xiao et al., 2020). Importantly, extracting and detecting genomic samples of Mtb in clinical settings poses challenges due to difficulties in obtaining sputum samples from the lower respiratory tract, particularly in children, as well as the need for specialized laboratories for nucleic acid extraction and detection procedures. Given these challenges, it is crucial to focus on key virulence factors, such as the 6-kDa early secreted antigen target (ESAT6) and 10-kDa culture filtrate protein (CFP10) proteins, which are critical to the pathogenesis and immune evasion mechanisms of live Mtb, and have been identified as molecular diagnostic biomarkers (Hamada et al., 2021). Therefore, our aim is to develop a novel aptamer molecular probe for CRISPR-based detection of live Mtb in a genome-free manner.

In this study, we employed the Magnetic bead Systematic Evolution of Ligands by Exponential Enrichment (SELEX) technique to isolate and optimize a novel 59 bp Aptamer 3 with high affinity for ESAT6 and CFP10 fusion proteins (EC). Furthermore, we designed a short complementary DNA blocker (21 bp) to create an Aptamer-blocker 3–7 (Ap-blocker 3–7) probe with Ap3 in vitro, which was subsequently integrated into the RPA process. The Ap-blocker 3–7 probe selectively binds to the EC protein in plasma samples, releasing a portion of the blockers. These released blockers subsequently hybridize with the remaining Aptamer-blockers and the residual Ap3, thereby enriching the complex into a fully double-stranded Aptamer (ds-Aptamer) through isothermal

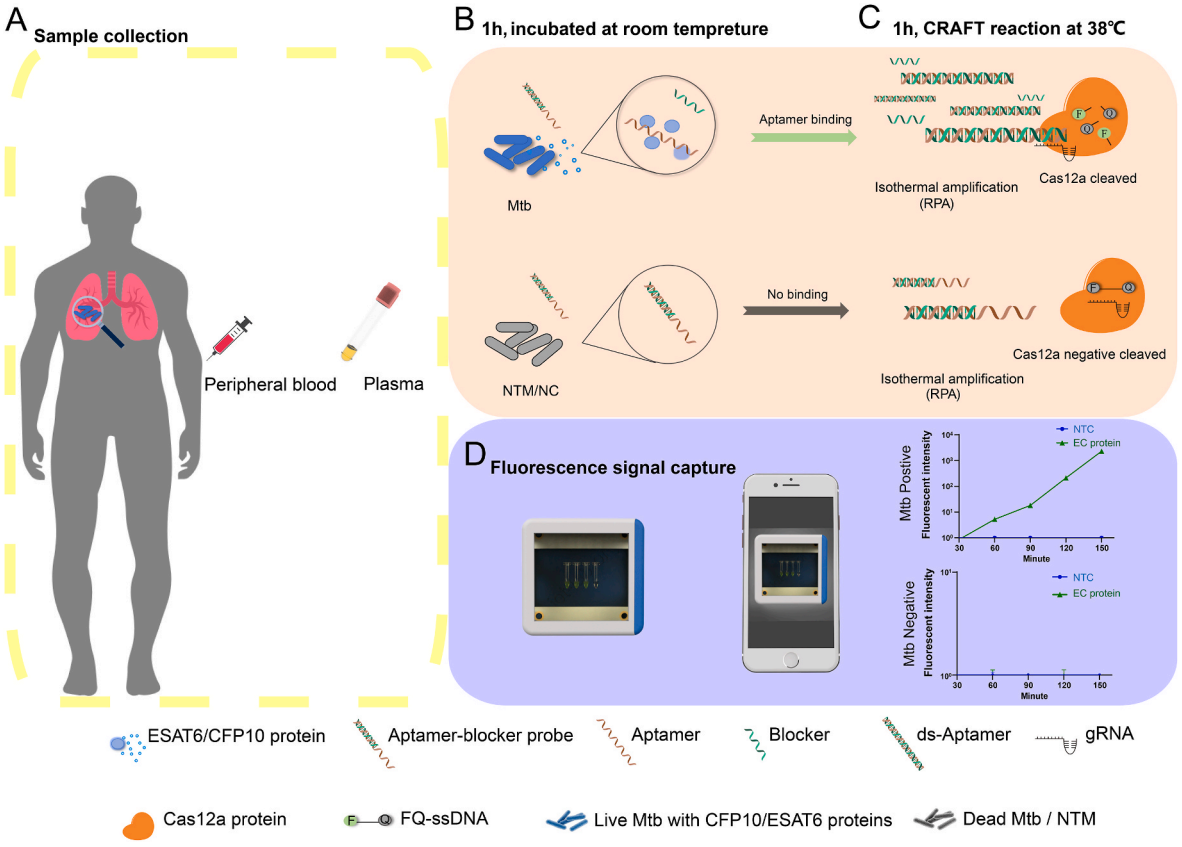


Fig. 1. Schematic of the workflow for detecting Live Mtb from Samples to Results. (A) Plasma samples were directly collected from clinical patients for immediate analysis. (B) The blocker single-stranded DNA (ssDNA) was released from the Aptamer-blocker probe in the presence of EC proteins secreted by live Mtb. In contrast, the blocker was not released in the presence of non-tuberculous mycobacteria (NTM) or in infections caused by dead Mtb. (C) The ssDNA blocker bound to the Aptamer-blocker probe and/or Aptamer, serving as a primer for isothermal amplification (RPA), which led to the amplification of double-stranded Aptamer (ds-Aptamer). Subsequently, the ds-Aptamer formed a ternary complex with Cas12a/gRNA, resulting in the cleavage of ssDNA fragments containing fluorophore-quencher (FQ-ssDNA). (D) This cleavage generated a fluorescent signal that could be read by a smartphone and analyzed using ImageJ software. The Aptamer-blocker probe exhibited limited capability in triggering the trans-cleavage of FQ-ssDNA by Cas12a, resulting in a negligible fluorescent signal as observed in the negative control (NTC). However, in the presence of EC protein, the Aptamer-blocker probe facilitated strong fluorescent signals through fragmentation amplification and Cas12a cleavage.

amplification. Subsequently, the ds-Aptamer forms a ternary complex with Cas12a/gRNA, resulting in the cleavage of FQ-ssDNA and the generation of a strong fluorescent signal.

2. Results

2.1. Aptamer-based CRISPR protocol for rapid detection of Live Mtb in plasma

An aptamer-based CRISPR protocol was developed and optimized to detect live Mtb directly from raw plasma samples within 120 min without nucleic acid extraction (Fig. 1A). Initially, aptamer-blocker probes were incubated with two plasma types at room temperature for 60 min. The probes bound to extracellular (EC) proteins secreted by live Mtb, triggering immediate blocker release (Fig. 1B). In contrast, no release occurred in plasma with nontuberculous mycobacteria (NTM) or dead Mtb due to absent EC protein secretion (Fig. 1B). Subsequently, A portion of the mixture was then transferred to a 0.2 mL tube containing the CRISPR/Cas12a system and recombinase polymerase amplification (RPA) components, followed by incubation at 38 °C for 60 min (Fig. 1C). Finally, fluorescence signals were captured using a smartphone camera, and ImageJ software was used to quantify intensity and classify samples as Mtb-positive or negative (Fig. 1D).

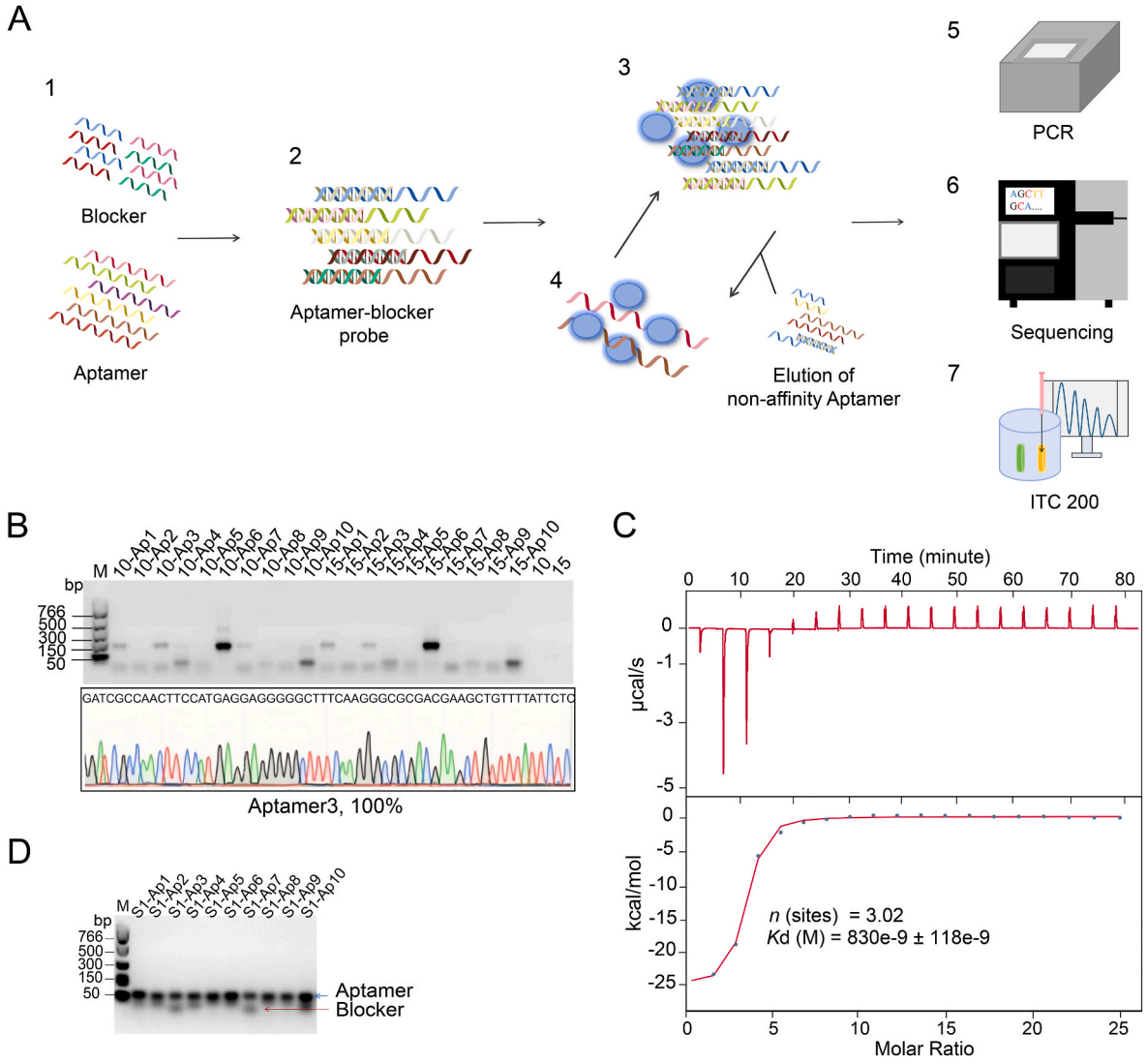


Fig. 2. Analysis of Aptamer and EC protein Binding Interactions Using Mag-beads SELEX. (A) Workflow of Mag-beads SELEX. 1. Designed ssDNA Aptamers and incomplete complementarity ssDNA blockers; 2. ssDNA Aptamer and ssDNA blockers hybridize individually to form Aptamer-blocker probes; 3. The Aptamer-blocker probe pool is mixed with magnetic bead-conjugated target protein; 4. Unbound Aptamers and blockers are eluted, followed by initiation of the next SELEX round with the existing mixture, continuing through the to fifteenth round; 5. The existing mixture and the eluents are identified by PCR after each round of Mag-beads SELEX; 6. The existing mixture is identified by Sanger sequencing following the Mag-beads SELEX; 7. Candidate Aptamer analysis is conducted with EC protein using Isothermal Titration Calorimetry (ITC). (B) Identification of Aptamer 1 to Aptamer 10 from the EC protein complex during the tenth and fifteenth rounds of EC protein-based SELEX using PCR. M: DNA ladder; 10-Ap1 to 10-Ap10, and 15-Ap1 to 15-Ap10 represent distinct sets of aptamers identified from the EC protein complex in the tenth and fifteenth rounds of SELEX, respectively. The amplified products of each aptamer were 144 bp in size, generated using Ap-F and Ap-R primers (Table S4). 10 and 15: amplicons from the EC protein complex in the tenth and fifteenth rounds of SELEX using primer-free PCR. (C) Calorimetric titration isotherms of the binding interactions between EC protein and Ap3. (D) Identify Aptamer 1 to Aptamer 10 and their corresponding blockers from the eluent of the EC protein in the first round of SELEX using PCR. S1-Ap1 to S1-Ap10 represent the amplicons of Aptamers (Ap1 to Ap10) and Blockers (blocker 1 to blocker 10) derived from the first round eluent in Mag-beads SELEX. The eluent S1 of SELEX was amplified using a single primer, as detailed in Table S4.

2.2. Aptamer 3 exhibited high affinity binding to the EC protein

To generate aptamers with high affinity for the EC protein, the Mag-beads SELEX method (Fig. 2A) was employed utilizing purified EC protein or Fetal Bovine plasma (FBS) as targets (Fig S1A, Fig S2A). The binding affinity of the aptamer-blocker pool increased with each selection round, peaking at the 15th round. Aptamer 1 (Ap1), Aptamer 3 (Ap3) and Aptamer 6 (Ap6), which demonstrated strong binding to the EC protein from the 15th selection complex and confirmed through Sanger sequencing (Fig. 2B, Fig. S1B). However, Ap1 and Ap6 also exhibited non-specific binding to FBS (Fig S2B, Fig S2C), while only Ap3 was identified in the final round of EC protein-based SELEX. The dissociation constant (*Kd*) of Ap3 was determined to be 8.30e10-7 M, with a binding stoichiometry (*N*) of 3.02, as established by isothermal titration calorimetry (ITC) one set of sites analysis model (Fig. 2C–Tables S5–S6). As shown in Fig. 2D and Fig. S1C, Aptamer-blocker 3–1 and Aptamer-blocker 7 released their blockers into the EC solution after the first SELEX round. This finding support the hypothesis that the Aptamer-blocker probe not only has the potential to bind to the EC protein complex but can also release the ssDNA blocker upon binding.

According to Fig. 3A and B, the truncation of the 5′ end by removing 21 nucleotides from the original sequence of Ap3 significantly impairs its binding affinity for the EC protein during the SELEX process. Specifically, retaining only the core 21-nucleotide sequence at the 5′ end results in a dramatic reduction of the *Kd* value to 1.81E-6 (Fig. S3). To further analyze the tolerance of Ap3 to amino acid mutations in the EC protein, we introduced mutations at six amino acid residues connected with Ap3 core sequence by hydrogen bonds (Fig. 3C), in addition to one conserved amino acid residue A84 present in MTB but mutated in NTM (Fig. 3D). Among these, the M1 and M2 proteins are located within the Esta 6 protein sequence, while the M3 and M4 mutants are situated in the CFP10 protein sequence (Tables S6–S7). One set of sites analysis model reveals that Ap3 did not exhibit a significant thermal response when titrating four EC mutants (Table S9). Interestingly, EC-M2 (A84Q) substituted only one conserved amino acid from MTB. It also exhibited no binding reaction with Ap3. This indicates that Ap3 exhibits high structural specificity for the EC protein and lacks affinity for mutations resulting from critical amino acid substitutions. All mutants also shown negative results in CRAFT (Fig. S5A).

2.3. CRISPR-driven aptamer fluorescence testing (CRAFT)

Double-stranded Ap3 (ds-Ap3) can be amplified using two primers through either Recombinase Polymerase Amplification (RPA) or PCR, which is subsequently visualized in a gel image (Fig. S4A). sgRNA targeting the ds-Ap3 amplicons was then selected to direct the Cas12a cleavage reaction. Three sgRNAs were designed, with Ap3-sg3 exhibiting the highest activity, as evidenced by the significant fluorescence signal ($P < 0.0001$) (Fig. 4A). In contrast, self-hybrid Ap3 (Ap3), Aptamer-blocker 3–1 probe (probe 3–1), and ssDNA Ap3 showed no positive signal in single Cas12a cleavage reaction (Fig. S4B–C). However, ssDNA blocker can facilitate RPA amplification when combined with Ap3 or probe 3–1 to form the ds-Ap3 (Fig. 4B). Surprisingly, the

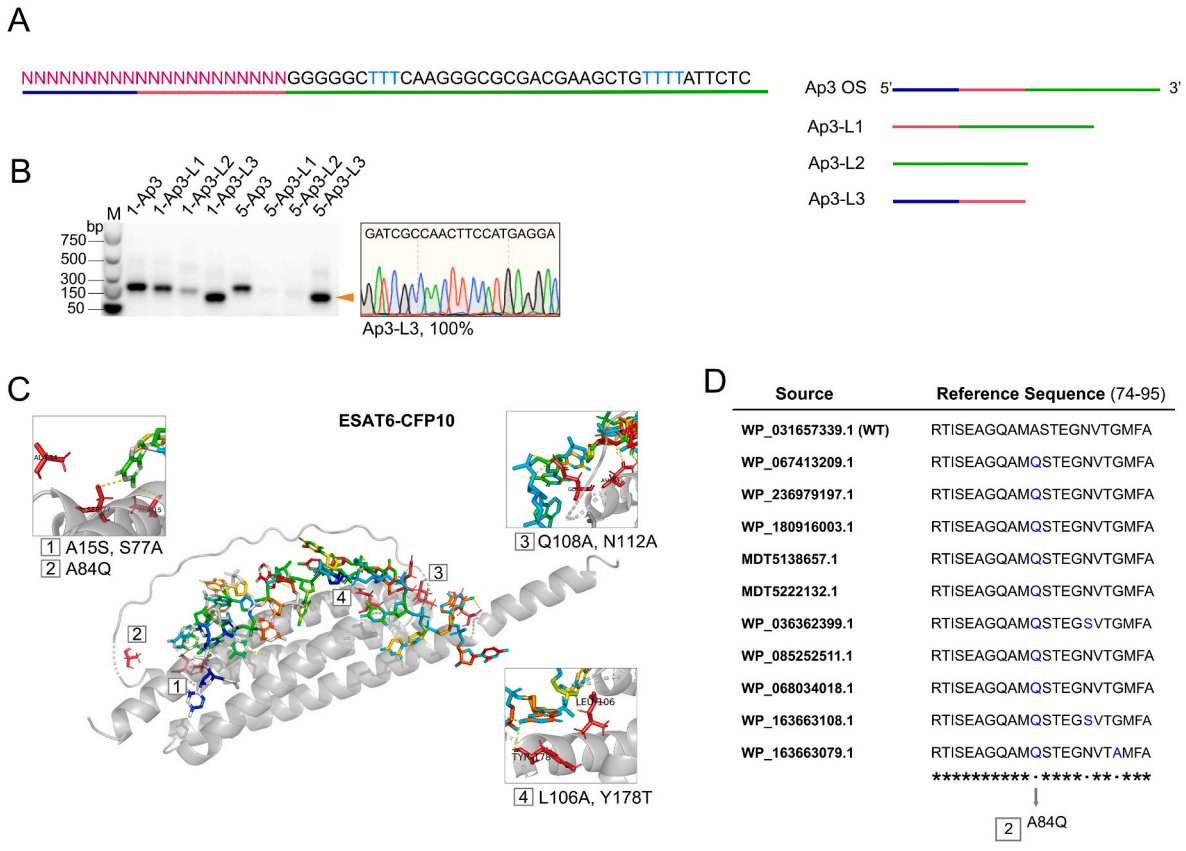


Fig. 3. Identification of the Interaction Motif Between Aptamer 3 and EC protein. (A) Truncated variants of Ap3 and Ap3 original sequence. The top panel shows the original sequence (OS) and mutant sequences (Ap3-L1 ~ Ap3-L3), with PAMs marked in blue. (B) Identification of Ap3-L1 to Ap3-L3 from the EC complex of EC-based SELEX using PCR and sanger sequencing. M: DNA ladder; 1-Ap3 to 15-Ap3-L3 represent distinct sets of aptamers identified from the EC protein complex in the first to fifteen rounds of SELEX, respectively. (C) 3D structure of EC protein and locations of amino acid substitutions in EC mutants. Hydrogen bonds between EC protein and Aptamer 3 interaction was marked as yellow dashed lines. Residues involved in hydrogen bond interactions are indicated in the zoomed-in diagram. (D) Comparison of conserved EC sequences between Mtb and 10 different NTM strains. Mutant amino acids in EC-M2 variant are marked in blue. Full source data are provided in Table S7 and TableS8.

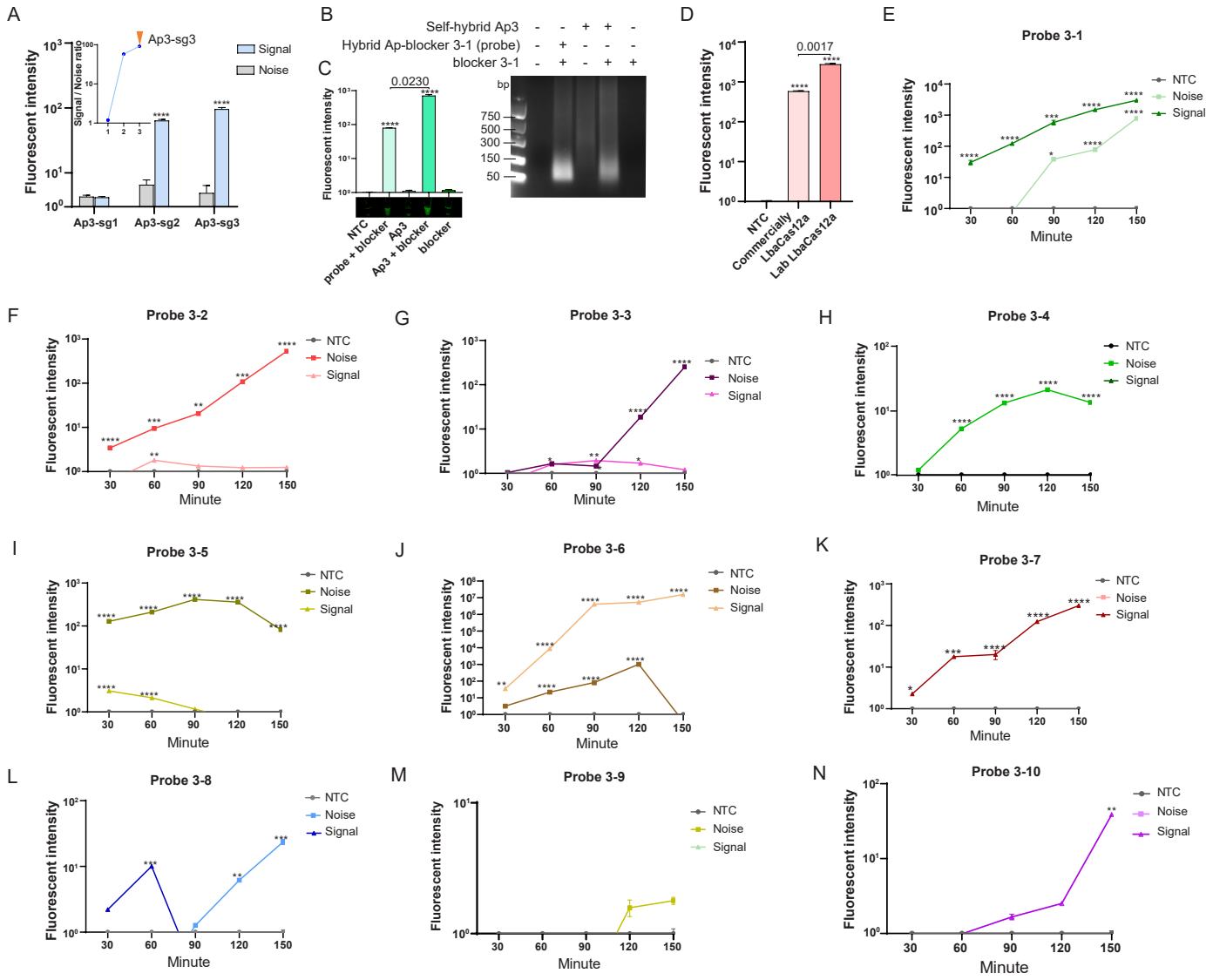


Fig. 4. Aptamer-blocker Probe Selection for Aptamer 3 via RPA-based CRISPR/Cas12a Fluorescence Detection. (A) Selection of sgRNA for the Cas12a system system using 10 μmol Ap3 PCR products as a template, reacting for 30 min at 37 °C. For the Signal group, the PCR products of Aptamer 3, amplified using Ap3-F and Ap3-R, were utilized as a template. For the Noise group, ddH2O was used as the template. The best sgRNA for ds-Ap3 identification is indicated by an orange triangle. (B) Gel image analysis of the amplicons from Self-Hybridized Aptamer 3, Aptamer-blocker 3–1 probe, and blocker 3–1 via RPA amplification. (C) Identification of self-hybrid Aptamer 3, Aptamer-blocker 3–1 and ssDNA blocker 3–1 using RPA-based CRISPR/Cas12a fluorescence detection in one pot, incubated for 30 min at 37 °C. (D) Comparison of Cas12a protein working efficiency between laboratory prepared and commercially proteins in Ap3 PCR products based fluorescence detection. (E–N) Comparative performance analysis of Aptamer-blocker 3–1 through Aptamer-blocker 3–10, with and without blocker 3–1 to blocker 3–10, over a duration of from 30 to 150 min. For the Signal group, 10 μmol Hybrid Ap-blocker probes plus 10 μmol ssDNA blockers was used as the template, and for the Noise group, Ap-blocker probes was used as the template. Error bars indicate standard errors of the mean (SEM) from three technical repetitions per group. Statistical significance is denoted as follows: $^{****}P < 0.0001$, $^{***}P < 0.001$, $^{**}P < 0.01$, $^{*}P < 0.05$, while non-marked values indicate no significant difference compare with the NTC.

primer-free RPA reaction can be integrated with the CRISPR reaction, allowing for the identification of Ap3 fluorescence in a single tube within 30 min (Fig. 4C). The results from the Western Blot (WB) indicate that the Cas12a protein, eluted from the prokaryotic expression system, exhibits exceptionally high purity (Fig. S4D). Following purification and collection, the protein concentration reaches 60 μg/mL. In subsequent co-reactions with RPA, the purified Cas12a protein demonstrated a significantly higher fluorescence value compared to the commercial control (Fig. 4D). To assess the stability of ssDNA within the co-reaction detection system utilizing the Aptamer-blocker probe as a template, we selected hybrid aptamer-blocker 3–7 (probe 3–7) from ten probes as the optimal one, which exhibited the greatest tolerance in RPA-based CRISPR/Cas12a fluorescence detection without EC protein (Fig. 4E–N). Crucially, probe 3–7 exhibited no false positive noise from self-detection, contrasting significantly with the interference observed from probe 3-1 during the detection process, spanning from 30 to 150 min (Fig.s. 4E and 5K).

Subsequently, we confirmed that probe 3–7 released bloker 3–7 upon interaction with the EC protein. Furthermore, bloker 3–7 was effectively employed as a primer to amplify Ap3 from the rest probe 3–7 or the EC pellet (Fig. 5A). Subsequent assessments revealed the release of blocker 3–7 into the EC soluble$^{probes\ 3\text{-}7}$, as evidenced by RPA-based CRISPR/Cas12a fluorescence detection (Fig. 5B). Notably, no positive signal was detected in the EC pellet$^{probes\ 3\text{-}7}$ and EC^{Ap3}, indicated the complete release of blocker 3–7 by probe 3–7 in the presence of EC (Fig. S5B). Thus, we named the program CRISPR-Driven Aptamer Fluorescence Testing (CRAFT).

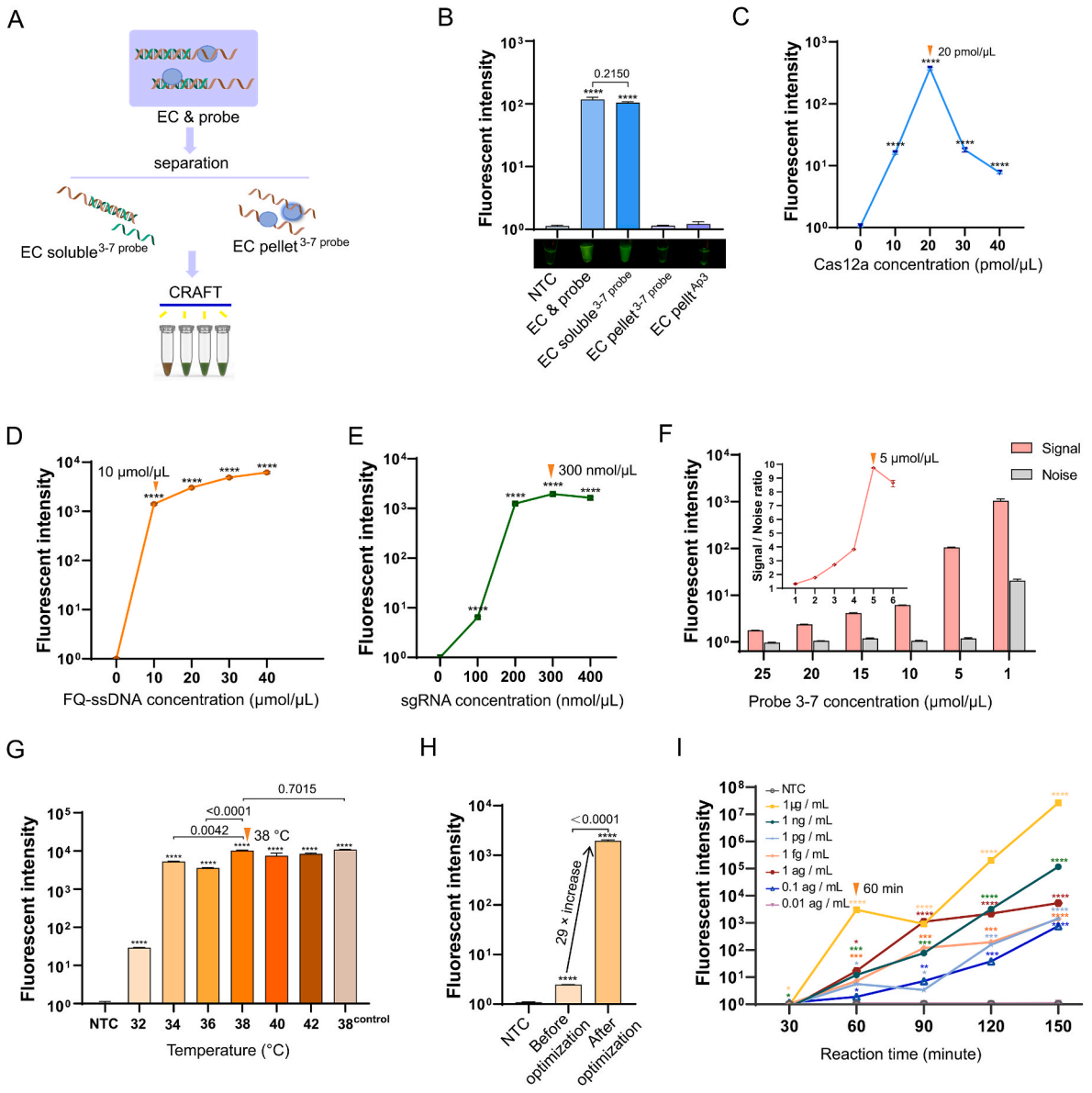


Fig. 5. Establishment and Optimization of the CRISPR-Driven Aptamer Fluorescence Testing (CRAFT). (A) Detection process of magnetic bead-conjugated EC protein by CRAFT. Magnetic bead-conjugated EC protein was incubated with Aptamer-blocker 3–7 probe (probe 3–7) for 1 h, and then separation to EC soluble$^{3\text{-}7\ probe}$ and EC pelelt$^{3\text{-}7\ probe}$ parts before CRAFT. (B) CRAFT results of the mixture of EC and 3–7 probes, EC soluble$^{3\text{-}7\ probe}$ and EC pelelt$^{3\text{-}7\ probe}$. For the negative control (NTC), the 100 ng/mL purified EC protein was used as the template. (C–E) Optimization the concentration of laboratory prepared LbaCas12a, FQ-ssDNA and sgRNA for CRAFT system. The best option for each optimization experiment is indicated by an orange triangle. (F) Concentration optimization of the probe 3–7 in CRAFT system. For the Signal group, the 100 ng purified EC protein was used as the template, and for the Noise group, ddH2O was used as the template. (G) Comparison of different reaction temperature for the CRAFT system using 5 μmol probe 3–7 plus 100 ng purified EC protein as a template, reacting for 30 min. NTC means none purified LbaCas12a added in the negative control, and 38^{control} means commercial LbaCas12a reaction result at 38 °C. (H) Comparison between CRAFT systems before and after optimizations for detecting EC protein. (I) EC protein-based LoD assay of the CRAFT system, reacting from 30 min to 150 min at 38 °C. Purified EC protein was diluted from 1 μg/mL to 0.01 ag/mL, equivalent to 3E10 EC protein particles per mL down to 0.3 EC protein particles per mL, with ddH2O utilized as the negative control (NTC). Error bars represent standard errors of the mean (SEM), three technical repetitions per group, $^{****}P < 0.0001$, $^{***}P < 0.001$, $^{**}P < 0.01$, $^{*}P < 0.05$, while non-marked values indicate no significant difference compare with the NTC.

2.4. Performance of CRAFT in sensitivity and specificity for Mtb diagnostic markers

The optimization of the CRAFT revealed that the most significant positive reaction occurred at a Cas12a concentration of 20 pmol, FQ-ssDNA concentration of 10 μmol, sgRNA concentration of 300 μmol, and probe 3–7 concentration of 5 μmol, and reaction temperature at 38 °C, as illustrated in Fig. 5C–G. After optimization of the above parameters, the final CRAFT system exhibited a 29 × increase in fluorescence intensity for the detection of the EC protein (Fig. 5H). To further determine the LoD of the optimized CRAFT system, we used it to detect 1 μg/mL of EC templates with dilute ranging from 1 μg/mL to 0.01 ag/mL. The result shown the sensitivity of CRAFT in detecting EC protein is 0.1 ag per mL, enabling the detection of as few as three EC protein particles in 1 mL of sample after just 60 min of incubation at 38 °C (Fig. 5I). This high sensitivity underscores the potential of CRAFT as a rapid and efficient diagnostic tool for identifying live Mtb biomarkers. Additionally, CRAFT demonstrated specificity in distinguishing between MTB (H37Ra) filtrate soluble, *Escherichia coli* (*E. coli*) filtrate, and human lung carcinoma cell line (A549) culture filtrate (Fig. 6A).

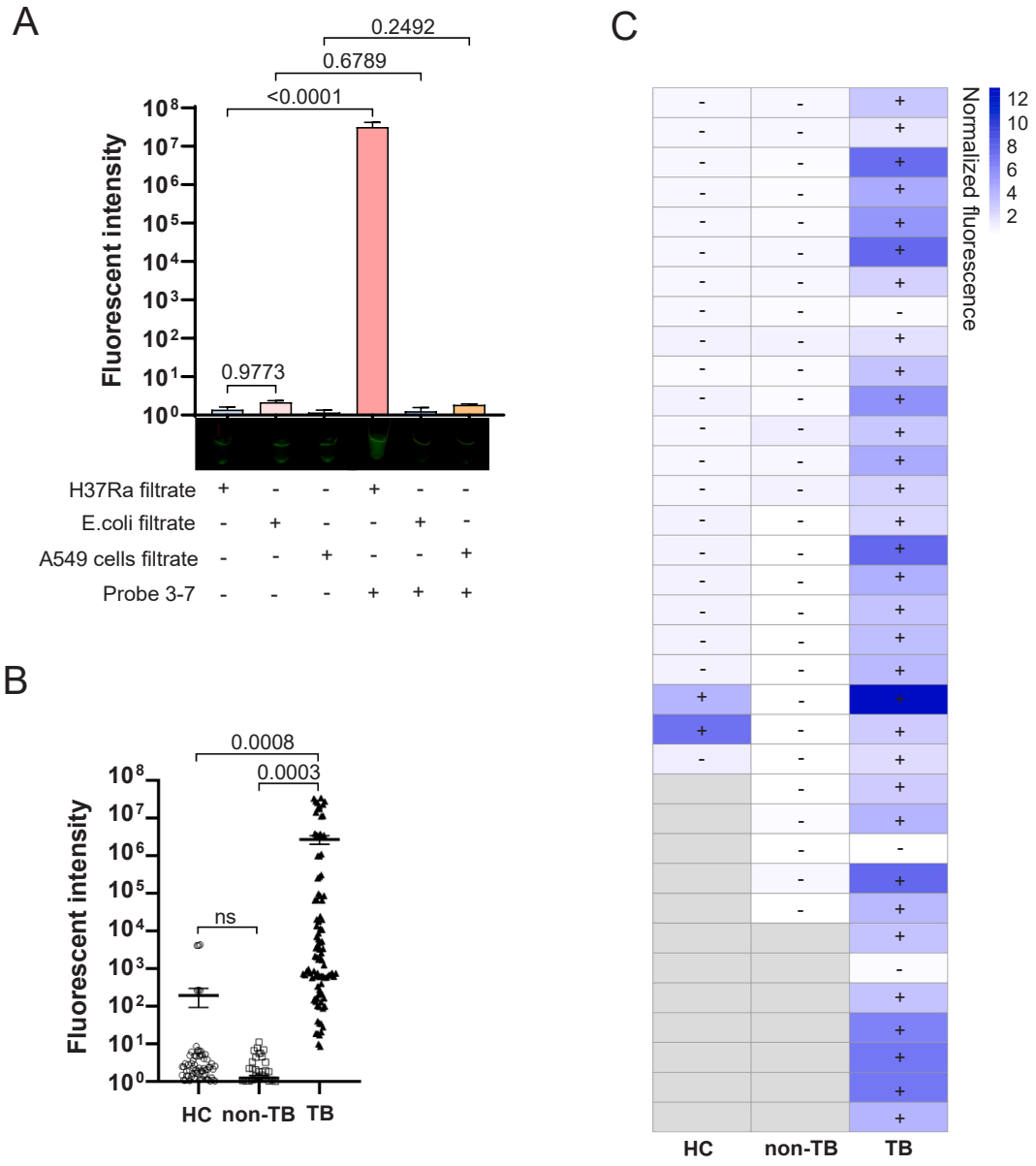


Fig. 6. Evaluation of the Sensitivity and Specificity of CRAFT. (A) Evaluation of the specificity of CRAFT using filtrates form H37Ra, *E. coli* and A549 cells. 1 mL filtrate were incubation with 5 μM Ap-blocker 3–7 probe for 1 h before CRAFT while negative control incubation with ddH_2O. Both bacterial strains were cultivated to an optical density (OD) of 0.62, while the proliferation of A549 cells reached a fusion degree of 80 %. Error bars represent standard errors of the mean (SEM), three technical repetitions per group, $^{****}P < 0.0001$, $^{***}P < 0.001$, $^{**}P < 0.01$, $^{*}P < 0.05$, while non-marked values indicate no significant difference compare with the NTC. (B) Evaluation of CRAFT on clinical samples. Error bars indicate the standard errors of the mean (SEM), with three technical replicates per sample. The fluorescence threshold for negative results is set at 10. (C) Fluorescence readouts of the CRAFT assay for the EC proteins performed on clinical samples. Plasma extracts from 35 positive patients (TB), 28 pulmonary or NTM infected patients (non-TB) and 23 healthy volunteers (HC) peripheral blood, determined by chest X-ray signs, molecular detection and clinical symptoms as described previously (2000; Rautman et al., 2024). Positive/Negative test interpretation is indicated by +/−.

2.5. Assessment of CRAFT for MTB diagnostic in clinical samples

To evaluate the performance of CRAFT using on human plasma samples from healthy individuals (HC), non-tuberculous *Mycobacteria* (NTM) plus pneumonia (PN) patients (none-TB), and tuberculosis patients (TB), a total of 86 plasma samples were analyzed. This included 35 samples that were confirmed as positive for tuberculosis via clinical laboratory tests and GeneXpert, while the remaining samples consisted of 5 NTM, 23 PN and 23 from chest X-ray negative plus IGRA negative individuals, as indicated in the assessment report (Table 1). Notably, no false positives were identified among the 5 NTM and 23 PN patients, which included 2 samples infected with *Mycobacterium abscessus*, 1 with *Mycobacterium intracellulare*, 1 with *Mycobacterium avium,* and 1 with *Mycobacterium kansasii* (Fig. 6B). A significant difference was observed between the healthy control (HC) group and the tuberculosis (TB) group ($P = 0.0008$), as well as between the non-TB group and the TB group ($P = 0.0003$) (Fig. 6B). However, no significant difference was noted between the HC group and the non-TB group. Nonetheless, three samples identified as Mtb positive by GeneXpert showed negative results in this study, while two samples classified as healthy exhibited positive Mtb signals in the CRAFT (Fig. 6C). The CRAFT results identified a sensitivity of 91.4 % (32 of 35) for chest X-ray positive TB cases and 96.4 % (27 of 28) for culture-positive TB cases. Additionally, the sensitivity for GeneXpert positive TB cases was 94.1 % (32 of 34). The sensitivity for smear microscopy positive and negative TB cases was 92.3 % (12 of 13) and 91 % (20 of 22), respectively. The CRAFT analyses also demonstrated a

Table 1
Sensitivity and specificity of CRAFT for TB diagnosis in clinical samples.

Clinical sample groups	Positive results/ total	Sensitivity, %	Specificity, %
HC (n = 23)			
Negative chest X-ray (23/23)	2/23		91.3 %
Negative IGRA (23/23)	2/23		91.3 %
non-TB (n = 28)			
PN (23/28)	0/23		100 %
NTM (5/28)	0/5		100 %
TB (n = 35)			
Positive chest X-ray (35/35)	32/35	91.4 %	
Positive culture (28/35)	27/28	96.4 %	
Positive GeneXpert (34/35)	32/34	94.1 %	
Positive smear microscopy (13/35)	12/13	92.3 %	

specificity of 91.3 % (2 of 23) for the HC group and 100 % (0 of 28) for non-TB subjects (Table 1).

3. Discussion

TB remains a major global health threat, claiming millions of lives annually. Despite ongoing efforts, the lack of rapid, accurate, and affordable diagnostic tools for live Mtb hampers effective treatment and control (Banoo et al., 2024). Distinguishing between live and dead Mtb presents substantial challenges for treatment monitoring, drug efficacy evaluation, and infections risk assessment, highlighting the urgent need for improved diagnostic methods (Ma et al., 2020; Tang et al., 2014).

Prominent diagnostic markers of Mtb, such as CFP10 and ESAT6, are abundantly present in fresh samples (Yang et al., 2015). Notably, these early secreted antigens are components of the EC protein complex, and play a crucial role during mycobacterial infection (Anes et al., 2023; Ramalingam et al., 2023), exhibiting high diagnostic value. Current diagnostic methods primarily rely on host immune responses, such as the Enzyme-linked Immunospot Assay (ELISpot) assay and Interferon-gamma Release Assays (IGRA), rather than directly detecting live Mtb, which leads to delays in diagnosis and treatment initiation (Pai et al., 2014). Traditional techniques, including ELISA and the Tuberculin Skin Test (TST), detect these proteins but require improvements in sensitivity and specificity, along with complex sample processing (Chandramuki et al., 2002). The low concentrations of EC proteins in plasma further complicate their detection (Laurentius et al., 2016). Recent advancements, such as a prototype bioelectronic TB antigen assay, show promise in rapid and conveniently detecting CFP10 in plasma and urine samples (Seifert et al., 2021; Wei et al., 2022), indicating the necessity for highly sensitive methods that efficiently capture and detect EC proteins in clinical settings.

In this study, the EC protein served as a standard biomarker for live Mtb(Chen et al., 2022), facilitating the development of an innovative detection method that integrates an aptamer-blocker probe and RPA-based CRISPR technologies. This method, named CRAFT (CRISPR-Driven Aptamer Fluorescence Testing), offers significant advantages in the detection of live Mtb. Furthermore, the Ap3 exhibited high specificity and affinity for the EC protein, while showing no significant affinity for EC mutants (as shown in Table S9), even with a single amino acid mutation (M2, Table S9). This approach is non-sputum based, requires no extraction, and allows for rapid and highly specific detection of EC proteins in plasma, thereby streamlining the diagnostic process and reducing costs in clinical settings. In the evaluation of CRAFT for Mtb diagnostics, using health clinical samples (Fig. 6C), two individuals showed positive results for live Mtb infection, potentially indicating early-stage tuberculosis. Conversely, among three individuals who tested negative for Mtb in CRAFT but positive in GeneXpert detection (Table 1), the possibility of dead Mtb infection exists, given GeneXpert's high sensitivity to Mtb nucleic acid but lack of specificity for distinguishing between live and dead Mtb(Park et al., 2024; Singh et al., 2024). Due to the source of health clinical samples from population-wide physical examinations, tracking and detecting the infection status for these individuals presents challenging. Further studies will continue to expand the time dimension.

Overall, the development of the CRAFT platform utilizing blood-based detection for live Mtb, holds significant promise for improving TB diagnostics, particularly in resource-limited settings. The integration of aptamers with CRISPR technology represents a novel approach for the sensitive and rapid detection of Mtb, which could substantially contribute to global TB control efforts. Future research will focus on exploring the application of CRAFT in point-of-care testing and its potential for detecting other pathogens, thereby increasing its clinical utility.

4. Materials and method

4.1. Clinical sample collection

From January 2024 to October 2024, participants were recruited from the Shenzhen Third Hospital (Shenzhen, China) (Table S1). The healthy control (HC) group consisted of 23 healthy adult participants who tested negative for Mtb using the IGRA and exhibited negative chest radiological signs. Additionally, 28 patients diagnosed with NTM or PN constituted the non-TB group. The non-TB group included 2 patients with *Mycobacterium abscessus*, 1 with *Mycobacterium intracellulare*, 1 with *Mycobacterium avium*, and 1 with *Mycobacterium kansasii*. The remaining PN patients were diagnosed based on clinical symptoms and radiological findings, as previously described (Rautman et al., 2024), and all had negative Mtb detection in sputum samples, indicated by culture and the GeneXpert method. Furthermore, 35 adults diagnosed with TB tested positive for Mtb using the GeneXpert or sputum culture or smear microscopy, along with the positive chest radiological signs and comorbidity assessment. All participants were confirmed to be HIV-negative. Demographic, microbiological, and diagnostic data are summarized in Table S2.

In total, 86 participants provided peripheral blood samples for our study. Each individual had 5 mL of peripheral blood drawn using a vacuum collection device (BD Vacutainer, USA). The plasma was then separated using centrifugation at 500×*g* for 5 min and transported at 4 °C. All fresh plasma samples were processed immediately upon collection. The study received approval from the Institutional Review Board of Shenzhen Third People's Hospital, and written informed consent was obtained from all participants.

4.2. Bacterial and cell culture conditions

The Mtb H37Rv strain was obtained from Shenzhen Third People's Hospital and cultured in Middlebrook 7H9 broth (Difco, USA) supplemented with 0.05 % Tween 80 and 10 % oleic acid, albumin, dextrose, and catalase (OADC), as previously describe (Guo et al., 2022). *Escherichia coli* (*E. coli*) was cultured in Luria-Bertani (LB) liquid medium at 37 °C with shaking at 180 rpm. Subsequently, the bacterial supernatants were collected by centrifugation at 3000 rpm for 3 min and filtered through a 0.22 μm membrane prior to analysis. The A549 cell line (Procell, China) was maintained in Dulbecco's Minimum Essential Medium (Gibco, China) supplemented with 10 % fetal bovine plasma (ExCell BIO, Uruguay) at 37 °C containing 5 % CO_2.

4.3. Aptamer probe

Ten ssDNA sequences were selected from a pool of 1000 ssDNA sequences, each containing a (5′-NNNNNNTTTNNNNNN-3′) PAM site at the 5′ or 3′ ends (Yamano et al., 2016) for sgRNA targeting, with each ssDNA being 59 nucleotides in length. These ssDNA aptamer sequences

were generated randomly online (https://www.detaibio.com/sms2/random_dna.html), and exhibited a folding conformation similar to that of the EC aptamer previously reported (Tang et al., 2014). Ten short ssDNA blockers, each complementary to 21 nucleotides of the corresponding aptamers, were designed and synthesized. All blocker and aptamer oligonucleotides (Table S3) were synthesized by Sangon Biotech and dissolved in sterile buffer before analysis. The 10 μM aptamer and 10 μM blocker hybridization reaction were incubated at 95 °C for 5 min and then allowed to anneal to room temperature overnight to form the respective aptamer-blocker probes. Self-hybridization of 10 μM Aptamer 3 was performed for the subsequent analysis of dissociation coefficients.

4.4. Magnetic bead SELEX

During the traditional SELEX process (Bock et al., 1992), a library of random sequence oligonucleotides undergoes iterative binding, separation, and amplification steps, resulting in the enrichment of aptamers with the desired binding properties. In the Mag-beads SELEX (Fig. S1), 100 μg of EC proteins and 200 μL of Fetal Bovine plasma (ExCell, China) were immobilized on the surface of magnetic-COOH beads (M2143, Solarbio) to form a target protein-bead complex according to the protocol. Subsequently, the hybridization library (10 μM for each aptamer-blocker dimer) was allowed to selectively interact with the targeted protein, and the mixture was fully mixed for 1 h at room temperature for each round, continuing up to the 15th round. Unbound aptamers and blockers were removed through magnetic separation, with the ssDNA blockers collected in the supernatant during rounds 1 to 15 of the selection process. Meanwhile, the ssDNA aptamers bound to the EC protein were recovered and amplified by PCR. Finally, the EC protein complexes were analyzed using PCR and Sanger sequencing. The candidate aptamers were subsequently verified for their dissociation constants with the EC protein using MicroCal PEAQ Isothermal Titration Calorimetry (ITC, Malvern, UK).

4.5. Isothermal titration analysis

To determine the dissociation constant (*K*d) and binding stoichiometry (*N*) of the interaction between the EC protein and Ap3, we employed MicroCal PEAQ ITC (Malvern Panalytical, UK) and following the previously reported method (Kamps et al., 2015). Both Ap3 and purified EC fusion proteins were prepared in identical solutions to eliminate heat changes arising from buffer mismatches. The ITC cell was loaded with the self-hybridized Ap3 at a concentration of 10 μM, while the syringe was filled with a 50 μM solution of EC protein. For the control, ITC cell was loaded with the protein buffer, while the syringe was filled with EC protein. During the titration, 2 μL of the syringe solution was injected into the protein cell at 25 °C, with a 250 s interval between each injection, and the heat changes from 19 injections were recorded. Heats of dilution for EC proteins were determined in control experiments, and were subtracted from the titration binding data before curve fitting. Data analysis was performed using the MicroCal PEAQ ITC software with one set of sites model, which generated a binding isotherm that was fitted to a binding model.

4.6. Proteins and western blot

For the expression, purification, and characterization of LbaCas12a, EC and its mutants (M1, M2, M3 and M4), plasmids encoding His-tagged proteins were transformed into *E. coli* BL21 cells. Cells was induced with 0.9 mM IPTG at 16 °C for 18 h, and then centrifuged to isolate cells pellet. Followed cells were lysed via sonication in lysis buffer (pH 8.0, 50 mM NaH2PO4, 300 mM NaCl and 10 mM imidazole) containing protease inhibitors (leupeptin and 0.1 mM PMSF). Lysates were clarified by centrifugation at 15,000×*g* for 15 min. Supernatants were loaded onto a HisPur Ni-NTA column (Smart-Lifesciences, China), washed with wash buffer (pH 8.0, 50 mM NaH2PO4, 300 mM NaCl and 25 mM imidazole), and eluted with elution buffer (pH 8.0, 50 mM NaH2PO4, 300 mM NaCl and 250 mM imidazole). Fractions were analyzed by SDS-PAGE (10 % gel) to assess purity. LbaCas12a and EC proteins were concentrated using a 100 kDa or 10 kDa centrifugal filter unit (Millipore, USA) respectively. Protein concentrations were determined using the BeyoBCA assay. For Western blot analysis, 20 μL of protein lysate was mixed with 5 × SDS (CWBIO, China), heated at 100 °C for 5 min, separated by SDS-PAGE, and transferred to NC membranes (Millipore, USA). Membranes were blocked in 5 % DifcoTM Skim milk (BD, USA) for 2 h at room temperature and then incubated with primary antibodies His-tag antibody (abcam, ab18184; 1:5000) overnight at 4 °C, followed by HRP-conjugated secondary antibodies (abcam, ab6728; 1:10000). Western blot were visualized using ECL reagents (Yeasen, China).

4.7. AlphaFold3 prediction and docking analysis

The Ap3 complex was first modeled using AlphaFold3 (https://alphafoldserver.com). Ap3 and EC protein complex docking was performed with AutoDOCK Vina (Ullah et al., 2024), using the core nucleic acid structure of Aptamer 3 (in this study) and the EC fusion protein (PDB: 1WA8). The sequences 1–21 of the Aptamer 3 were defined as active as they were involved in the interaction between Aptamer 3 and EC residues in both AlphaFold3 prediction model and mutation analysis (Fig. 4C). As a representative structure of the Ap3-EC complex was selected from the top six clusters based on AutoDOCK scoring. The nucleic acid-protein interactions were analyzed and visualized using PyMOL software.

4.8. In vitro transcription

For the preparation of gRNA, transcription templates Ap3-sg1, Ap3-sg2, and Ap3-sg3 targeting ds-aptmer03 were designed using CRISPR-offinder software as previously described (Liu et al., 2021). Subsequently, Ap3-sg1, Ap3-sg2, and Ap3-sg3 were amplified from a T7-promoter plasmid using the primer pairs listed in Table S4, following the LAmp Master Mix (P312−01, Vazyme) protocol. The purified PCR amplicons served as the DNA template for in vitro transcription (IVT) reactions utilizing the HiScribe T7 High Yield RNA Synthesis Kit (E2040S, NEB) at 37 °C overnight. To eliminate any residual transcription templates, 1 U of DNase I (EN0521, Thermo Fisher Scientific) was included in each IVT reaction. Following the purification of the gRNA fragments using the Monarch RNA Cleanup Kit (T2040L, NEB), each gRNA was quantified for quality and concentration using gel electrophoresis and a NanoDrop One spectrophotometer (Thermo Fisher Scientific).

4.9. Recombinase polymerase amplification (RPA) and polymerase chain reaction (PCR)

RPA reactions were conducted in a 96-well dry bath (TIANGEN) at 38 °C for 30 min, adhering to the protocol of the DNA Basis Kit (WLRB8201KIT, AMP-Future Biotech). Subsequently, the RPA products were purified using the DNA Clean-Up Kit (D4017, Zymo Research) prior to gel imaging. All PCR reactions were performed in a 96-well thermal cycler PCR system (Thermo Fisher Scientific) according to the amplification protocols: an initial denaturation at 95 °C for 5 min, followed by 35 cycles of denaturation at 95 °C for 30 s, annealing at 55 °C for 30 s, extension at 72 °C for 10 s, and a final extension at 72 °C for 5 min. The 2 × LAmp Master Mix (P312-01, Vazyme) was utilized in this study, and all primer pairs employed in the PCR reactions are listed in Table S4 of the supplementary information. The amplification of all amplicons was confirmed by agarose gel electrophoresis using 8 μL of each sample.

4.10. CRISPR-driven aptamer fluorescence testing (CRAFT)

The EC protein was obtained from Gene Optimal and diluted from 100 μg/mL to 0.01 ag/mL, corresponding to a range from 3×10^{15} particles of EC protein to 0.3 particles. Concentrations of 1 μg/mL, 1 ng/mL, 1 pg/mL, 1 fg/mL, 1 ag/mL, 0.1 ag/mL, and 0.01 ag/mL of the EC protein were subsequently analyzed using RPA-based CRISPR/Cas12a fluorescence detection. A 5 μM Ap-blocker 3–7 probe was thoroughly mixed with 1 mL of EC protein at room temperature for 1 h, with self-mixed Ap3 serving as the negative control. Following this, take 20 μl of the Ap-blocker 3–7 probe and sample mixture was combined with the RPA-based CRISPR/Cas12a systems (WLRB8201KIT, AMP-Future Biotech), which included 300 nM gRNA, 20 *p*M Cas12a, and 30 μM FQ-ssDNA, in a new reaction tube. All nucleic acid sequences and FQ-ssDNA are listed in Table S4. Sterile water was added to achieve a final reaction volume of 30 μL, and the mixture was incubated at 38 °C for an additional hour. The reaction tubes were then placed under a blue light illuminator to visualize the green fluorescence signals indicative of Mtb detection. The fluorescence intensity of each reaction was captured by a smartphone over a period of 30–150 min and quantified using ImageJ software. Fresh plasma clinical samples were collected from non-TB patients, TB patients, and healthy controls, with 500 μL of plasma mixed with 10 μM Ap-blocker 3–7 probe for the detection of Mtb in this study.

4.11. Statistical analysis

Data were analyzed using Graph-Pad Prism 8.0.1. Fluorescent intensity analysis employed a one-way ANOVA for comparisons involving three or more groups, while an unpaired *t*-test was utilized for comparisons between two groups, with SEM representing the standard error of the mean. Significant differences were determined by comparison to the negative control group, with significance levels indicated as follows: ****P value < 0.0001, ***$P < 0.001$, **$P < 0.01$, *$P < 0.05$. P value greater than 0.05 were considered non-significant.

CRediT authorship contribution statement

Siyuan Liu: Writing – review & editing, Writing – original draft, Validation. **Guohui Xiao:** Data curation. **Peixuan Li:** Validation. **Yating Xu:** Visualization. **Xinhao Fan:** Visualization. **Lin Tian:** Data curation. **Su Zhang:** Data curation. **Guoliang Zhang:** Writing – review & editing, Writing – original draft, Resources.

Declaration of competing interest

The authors declare that they have no competing interests. All authors have approved the submission of the manuscript to your esteemed journal. The content of the manuscript has not been published or submitted for publication elsewhere.

Acknowledgments

This work was supported by the National Key Research and Development Plan (No. 2020YFA0907201), the National Natural Science Foundation of China (No. 82370012), the Guangdong Science Fund for Distinguished Young Scholars (No. 0620220214), the Shenzhen Scientific and Technological Foundation (No. KCXFZ20211020163545004, RCJC20221008092726022), the Sanming Project of Medicine in Shenzhen (No. SZZYSM202311009), the Major Project of Guangzhou National Laboratory (No. GZNL 2024A01009), and the Shenzhen High-level Hospital Construction Fund.

Appendix A. Supplementary data

Supplementary data to this article can be found online at https://doi.org/10.1016/j.bios.2025.117566.

Data availability

Data will be made available on request.

References

Acquah, C., Agyei, D., Obeng, E.M., Pan, S., Tan, K.X., Danquah, M.K., 2020. Aptamers: an emerging class of bioaffinity ligands in bioactive peptide applications. Crit. Rev. Food. Sci. 60 (7), 1195–1206.
Ai, J.W., Zhou, X., Xu, T., Yang, M., Chen, Y., He, G.Q., Pan, N., Cai, Y., Li, Y., Wang, X., Su, H., Wang, T., Zeng, W., Zhang, W.H., 2019. CRISPR-Based rapid and ultra-sensitive diagnostic test for Mycobacterium tuberculosis. Emerg. Microb. Infect. 8 (1), 1361–1369.
Anes, E., Pires, D., Mandal, M., Azevedo-Pereira, J.M., 2023. ESAT-6 a major virulence factor of Mycobacterium tuberculosis. Biomolecules 13 (6), 968.
Bagcchi, S., 2023. WHO's global tuberculosis report 2022. Lancet Microbe 4 (1), e20.
Banoo, S., Yadav, Y., Tyagi, R., Manna, A., Sagar, R., 2024. Recent efforts in the development of glycoconjugate vaccine and available treatment for tuberculosis. Bioogr. Chem. 150 (1), 107610.
Bock, L.C., Griffin, L.C., Latham, J.A., Vermaas, E.H., Toole, J.J., 1992. Selection of single-stranded DNA molecules that bind and inhibit human thrombin. Nature 355 (6360), 564–566.
Boehme, C.C., Nabeta, P., Hillemann, D., Nicol, M.P., Shenai, S., Krapp, F., Allen, J., Tahirli, R., Blakemore, R., Rustomjee, R., Milovic, A., Jones, M., O'Brien, S.M., Persing, D.H., Ruesch-Gerdes, S., Gotuzzo, E., Rodrigues, C., Alland, D., Perkins, M. D., 2010. Rapid molecular detection of tuberculosis and rifampin resistance. N. Engl. J. Med. 363 (11), 1005–1015.
Boehme, C.C., Nicol, M.P., Nabeta, P., Michael, J.S., Gotuzzo, E., Tahirli, R., Gler, M.T., Blakemore, R., Worodria, W., Gray, C., Huang, L., Caceres, T., Mehdiyev, R., Raymond, L., Whitelaw, A., Sagadevan, K., Alexander, H., Albert, H., Cobelens, F., Cox, H., Alland, D., Perkins, M.D., 2011. Feasibility, diagnostic accuracy, and effectiveness of decentralised use of the xpert MTB/RIF test for diagnosis of tuberculosis and multidrug resistance: a multicentre implementation study. Lancet 377 (9776), 1495–1505.
Broughton, J.P., Deng, X., Yu, G., Fasching, C.L., Servellita, V., Singh, J., Miao, X., Streithorst, J.A., Granados, A., Sotomayor-Gonzalez, A., Zorn, K., Gopez, A., Hsu, E., Gu, W., Miller, S., Pan, C.Y., Guevara, H., Wadford, D.A., Chen, J.S., Chiu, C.Y., 2020. CRISPR-Cas12-based detection of SARS-CoV-2. Nat. Biotechnol. 38 (7), 870–874.
Chandramuki, A., Lyashchenko, K., Kumari, H.B., Khanna, N., Brusasca, P., Gourie-Devi, M., Satishchandra, P., Shankar, S.K., Ravi, V., Alcabes, P., Kanaujia, G.V., Gennaro, M.L., 2002. Detection of antibody to Mycobacterium tuberculosis protein antigens in the cerebrospinal fluid of patients with tuberculous meningitis. J. Infect. Dis. 186 (5), 678–683.
Chen, H., Li, S., Zhao, W., Deng, J., Yan, Z., Zhang, T., Wen, S.A., Guo, H., Li, L., Yuan, J., Zhang, H., Ma, L., Zheng, J., Gao, M., Pang, Y., 2022. A peptidomic approach to identify novel antigen biomarkers for the diagnosis of tuberculosis. Infect. Drug Resist. 15 (1), 4617–4626.
Denkinger, C.M., Schumacher, S.G., Boehme, C.C., Dendukuri, N., Pai, M., Steingart, K. R., 2014. Xpert MTB/RIF assay for the diagnosis of extrapulmonary tuberculosis: a systematic review and meta-analysis. Eur. Respir. J. 44 (2), 435–446.
Ehrt, S., Schnappinger, D., Rhee, K.Y., 2018. Metabolic principles of persistence and pathogenicity in Mycobacterium tuberculosis. Nat. Rev. Microbiol. 16 (8), 496–507.
Gootenberg, J.S., Abudayyeh, O.O., Lee, J.W., Essletzbichler, P., Dy, A.J., Joung, J., Verdine, V., Donghia, N., Daringer, N.M., Freije, C.A., Myhrvold, C., Bhattacharyya, R.P., Livny, J., Regev, A., Koonin, E.V., Hung, D.T., Sabeti, P.C., Collins, J.J., Zhang, F., 2017. Nucleic acid detection with CRISPR-Cas13a/C2c2. Science 356 (6336), 438–442.
Guo, Q., Bi, J., Lin, Q., Ye, T., Wang, Z., Wang, Z., Liu, L., Zhang, G., 2022. Whole genome sequencing identifies novel mutations associated with bedaquiline resistance in Mycobacterium tuberculosis. Front. Cell. Infect. Microbiol. 12.
Hamada, Y., Cirillo, D.M., Matteelli, A., Penn-Nicholson, A., Rangaka, M.X., Ruhwald, M., 2021. Tests for tuberculosis infection: landscape analysis. Eur. Respir. J. 58 (5), 2100167.
Joung, J., Ladha, A., Saito, M., Kim, N.G., Woolley, A.E., Segel, M., Barretto, R., Ranu, A., Macrae, R.K., Faure, G., Ioannidi, E.I., Krajeski, R.N., Bruneau, R., Huang, M.W., Yu, X.G., Li, J.Z., Walker, B.D., Hung, D.T., Greninger, A.L., Jerome, K.R., Gootenberg, J.S., Abudayyeh, O.O., Zhang, F., 2020. Detection of SARS-CoV-2 with SHERLOCK one-pot testing. N. Engl. J. Med. 383 (15), 1492–1494.
Kamps, J.J., Huang, J., Poater, J., Xu, C., Pieters, B.J., Dong, A., Min, J., Sherman, W., Beuming, T., Matthias, B.F., Li, H., Mecinovic, J., 2015. Chemical basis for the recognition of trimethyllysine by epigenetic reader proteins. Nat. Commun. 6, 8911.
Labib, M., Zamay, A.S., Kolovskaya, O.S., Reshetneva, I.T., Zamay, G.S., Kibbee, R.J., Sattar, S.A., Zamay, T.N., Berezovski, M.V., 2012. Aptamer-based viability impedimetric sensor for bacteria. Anal. Chem. 84 (21), 8966–8969.
Laurentius, L.B., Crawford, A.C., Mulvihill, T.S., Granger, J.H., Robinson, R., Spencer, J. S., Chatterjee, D., Hanson, K.E., Porter, M.D., 2016. Importance of specimen pretreatment for the low-level detection of mycobacterial lipoarabinomannan in human serum. Analyst 142 (1), 177–185.
Li, N., Huang, X., Sun, D., Yu, W., Tan, W., Luo, Z., Chen, Z., 2018. Dual-aptamer-based voltammetric biosensor for the Mycobacterium tuberculosis antigen MPT64 by using a gold electrode modified with a peroxidase loaded composite consisting of gold

nanoparticles and a Zr(IV)/terephthalate metal-organic framework. Microchim. Acta 185 (543).
Liu, S., Tao, D., Liao, Y., Yang, Y., Sun, S., Zhao, Y., Yang, P., Tang, Y., Chen, B., Liu, Y., Xie, S., Tang, Z., 2021. Highly sensitive CRISPR/Cas12a-Based fluorescence detection of porcine reproductive and respiratory syndrome virus. ACS Synth. Biol. 10 (10), 2499–2507.
Ma, Z., Ji, X., Yang, H., He, J., Zhang, Q., Wang, Y., Wang, Z., Chen, C., 2020. Screening and evaluation of Mycobacterium tuberculosis diagnostic antigens. Eur. J. Clin. Microbiol. 39 (10), 1959–1970.
MacLean, E., Kohli, M., Weber, S.F., Suresh, A., Schumacher, S.G., Denkinger, C.M., Pai, M., 2020. Advances in molecular diagnosis of tuberculosis. J. Clin. Microbol. 58 (10).
Pai, M., Denkinger, C.M., Kik, S.V., Rangaka, M.X., Zwerling, A., Oxlade, O., Metcalfe, J. Z., Cattamanchi, A., Dowdy, D.W., Dheda, K., Banaei, N., 2014. Gamma interferon release assays for detection of Mycobacterium tuberculosis infection. Clin. Microbiol. Rev. 27 (1), 3–20.
Park, M., Kumar, K., Coleman, M., Martin, L., Russell, G., Scheelbeek, P., Lalvani, A., Satta, G., Kon, O.M., 2024. TB PCR in BAL and EBUS-TBNA samples for the diagnosis of pulmonary and mediastinal lymph node TB: retrospective TRiBE study. Thorax 79, 870–877.
Ramalingam, G., Jayaraman, S., Khan, J.M., Ahmed, M.Z., Ahmad, A., Manickan, E., Rajagopal, P., 2023. Exploring recombinant secretory proteins from Mycobacterium tuberculosis to develop a serological platform for tuberculosis diagnosis. Int. J. Biol. Macromol. 249, 126769.
Rautman, L.H., Kammerer, J.S., Silk, B.J., Marconi, V.C., Youngblood, M.E., Edwards, J. A., Wortham, J.M., Self, J.L., 2024. Characteristics of TB cases without documented sputum culture in the United States, 2011-2021. Int. J. Tubercul. Lung Dis. 28 (5), 231–236.
Seifert, M., Vargas, E., Ruiz-Valdepenas, M.V., Wang, J., Rodwell, T.C., Catanzaro, A., 2021. Detection and quantification of Mycobacterium tuberculosis antigen CFP10 in serum and urine for the rapid diagnosis of active tuberculosis disease. Sci. Rep. 11 (1), 19193.
Shi, T., Jiang, P., Peng, W., Meng, Y., Ying, B., Chen, P., 2024. Nucleic acid and nanomaterial synergistic amplification enables dual targets of ultrasensitive fluorescence quantification to improve the efficacy of clinical tuberculosis diagnosis. Acs. Appl. Mater. Inter. 16 (12), 14510–14519.
Singh, U.B., Singh, M., Rodrigues, C., Christopher, D.J., Mahajan, N., Srivastav, A., Singh, K.J., Kanswal, S., Rao, M., Kazi, M., Sawant, D., Thangakunam, B., Vijay, C.V., Shankar, D., Bhatnagar, A., Mohan, A., Ahuja, V., 2024. Multi-centric evaluation of truenat MTB and MTB-RIF Dx assays for diagnosis of extrapulmonary tuberculosis. Sci. Rep. 14 (1), 15680.
Song, Y., Zhu, Z., An, Y., Zhang, W., Zhang, H., Liu, D., Yu, C., Duan, W., Yang, C.J., 2013. Selection of DNA aptamers against epithelial cell adhesion molecule for cancer cell imaging and circulating tumor cell capture. Anal. Chem. 85 (8), 4141–4149.
Tang, X.L., Zhou, Y.X., Wu, S.M., Pan, Q., Xia, B., Zhang, X.L., 2014. CFP10 and ESAT6 aptamers as effective mycobacterial antigen diagnostic reagents. J. Infect. 69 (6), 569–580.
Tian, Z., Yan, H., Zeng, Y., 2024. Solid-phase extraction and enhanced amplification-free detection of pathogens integrated by multifunctional CRISPR-Cas12a. Acs. Appl. Mater. Inter. 16 (12), 14445–14456.
Ullah, H., Majid, S., Abro, A., Rahman, T.U., Khan, A.M., Ahmed, M., Asif, M., Yousafzai, A., Ullh, R., Pushparaj, P.N., Rasool, M., 2024. Synthesis and molecular docking analysis of MBH adducts' derived amides as potential beta-lactamase inhibitors. Bioinformation 20 (5), 449–459.
Vinkenborg, J.L., Karnowski, N., Famulok, M., 2011. Aptamers for allosteric regulation. Nat. Chem. Biol. 7 (8), 519–527.
Wei, Y., Tao, Z., Wan, L., Zong, C., Wu, J., Tan, X., Wang, B., Guo, Z., Zhang, L., Yuan, H., Wang, P., Yang, Z., Wan, Y., 2022. Aptamer-based Cas14a1 biosensor for amplification-free live pathogenic detection. Biosens. Bioelectron. 211, 114282.
Xiao, G., He, X., Zhang, S., Liu, Y., Liang, Z., Liu, H., Zhang, J., Ou, M., Cai, S., Lai, W., Zhang, T., Ren, L., Zhang, G., 2020. Cas12a/Guide RNA-based platform for rapid and accurate identification of major mycobacterium species. J. Clin. Microbiol. 58 (2).
Yamano, T., Nishimasu, H., Zetsche, B., Hirano, H., Slaymaker, I.M., Li, Y., Fedorova, I., Nakane, T., Makarova, K.S., Koonin, E.V., Ishitani, R., Zhang, F., Nureki, O., 2016. Crystal structure of Cpf1 in complex with guide RNA and target DNA. Cell 165 (4), 949–962.
Yang, H., Li, A., Dang, L., Kang, T., Ren, F., Ma, J., Zhou, Y., Yang, Y., Lei, J., Zhang, T., 2023a. A rapid, accurate, and low-cost method for detecting Mycobacterium tuberculosis and its drug-resistant genes in pulmonary tuberculosis: applications of MassARRAY DNA mass spectrometry. Front. Microbiol. 14, 1093745.
Yang, H., Zhang, Y., Teng, X., Hou, H., Deng, R., Li, J., 2023b. CRISPR-based nucleic acid diagnostics for pathogens. Trac-Trend. Anal. Chem. 160, 116980.
Yang, Y., Mu, J., Chen, G., Zhan, Y., Zhong, J., Wei, Y., Cheng, K., Qin, B., You, H., Xie, P., 2015. iTRAQ-based quantitative proteomic analysis of cerebrospinal fluid reveals NELL2 as a potential diagnostic biomarker of tuberculous meningitis. Int. J. Mol. Med. 35 (5), 1323–1332.